FREQUENCY-DOMAIN ANALYSIS OF OFFSHORE PLATFORM IN NON-GAUSSIAN SEAS

By Ahsan Kareem,[1] C. C. Hsieh,[2] and M. A. Tognarelli[3]

ABSTRACT: A frequency-domain solution approach for the response of a system whose inputs are nonlinear transformations of non-Gaussian (nonlinear) wave kinematic processes is introduced. Particularly, this paper compares the probabilistic response characteristics of jacket-type platforms in deep water that are subjected to both Gaussian and non-Gaussian random wave loadings. Unlike earlier analytical treatments of this class of system, a statistical description of the wave forces is first developed to reflect nonlinearities and associated non-Gaussianity in the wave field kinematics. The kinematics are derived from Laplace's equation and nonlinear boundary conditions using a second-order Stokes' perturbation expansion. The deck response resulting particularly because of the effects of the second-order contribution to the loads on an idealized platform is computed. Consideration is given to the importance of the spacing of the legs to the response of the structure. The impact of swell in addition to locally wind-generated waves also is assessed. Ignoring the nonlinearity of the waves results in underestimation of the response level for all scenarios considered.

INTRODUCTION

Deepwater drilling efforts expose offshore platforms to an increasingly more hostile ocean environment. For jacket-type platforms designed for deep water, static or quasi-static analysis is not as realistic as it is for shallower depths. Reliable response analysis and design of these platforms can be ensured only through an improved understanding of environmental load effects, especially those resulting from wave hydrodynamics. Most studies on the dynamic analysis of offshore structures in deep water have been based on linear wave theory because it provides a satisfactory approximation to the wave kinematics of a Gaussian random sea state. Nevertheless, departure of the free-surface elevation from Gaussianity, reflecting the nonlinearities of the sea waves, has been observed (e.g., Spidsøe and Hilmarsen 1983; Marthinsen and Winterstein 1992). This paper employs previously developed statistics of non-Gaussian wave kinematics derived from second-order Stokes' random wave theory in, e.g., Kareem and Hsieh (1991); and Kareem et al. (1994, 1996) and investigates their effect on platform root-mean square (RMS) response statistics using the relative motion form of the Morison drag force, which is nonlinear in terms of both platform and water-particle velocity, as the system input (Chakrabarti 1987). JONSWAP and Ochi-Hubble spectra are used to model the linear random wave fields. Although both models include the effects of locally wind-generated waves, the Ochi-Hubble spectrum additionally includes the effects of low-frequency swells. Tayfun (1990) has suggested that the high-frequency attenuation of these spectra indicates that they include nonlinear effects and that a filtering approach should be used to arrive at more appropriate linear wave field spectra. This will be a subject of future consideration within the framework outlined here. The dynamic response analysis of the jacket-type platform is performed utilizing a frequency-domain approach, which offers computational efficiency.

Initially, the nonlinearity of the drag force precluded development of a frequency-domain-based analysis procedure to analyze the random wave load effects on jacket-type platforms, even in the case of a linear wave field. Borgman (1967) introduced enhancements to linearization and made it possible to establish a spectral description of the drag force by a series of convolutions involving water-particle velocity spectra. Investigations of the dynamics of jacket-type offshore platforms indicated that the quadratic dependence of the drag force on the water-particle velocity led to significant excitation near one of the platform resonant frequencies (for the platform in question, three times the dominant wave frequency) and thus caused an appreciable increase in the platform response—a phenomenon that is ignored within the framework of the stochastic linearization technique (Eatock-Taylor and Rajagopalan 1982; Rajagopalan and Eatock-Taylor 1982). Several others have presented different schemes to address the nonlinearity of the drag force as well as effects of intermittent wave action (e.g., Tung 1975; Borgman 1982; Gudmestad and Connor 1983; Deleuil et al. 1986; Lipsett 1986; Spanos and Donley 1990; Kareem and Li 1992; Kareem and Zhao 1994; Kareem et al. 1995; Tognarelli et al. 1997; Naess and Yim 1996).

The leg configuration of a jacket-type platform and the incident wave field can be such that the wave forces on the legs nearly cancel one another, resulting in minimal dynamic response. In the real ocean environment, the randomness of waves makes it difficult to evaluate the effectiveness of wave force cancellation in a straightforward manner. Here, then, it is desirable to examine the level of wave cancellation in a random wave field.

STATISTICS OF WAVE FORCE

Under general conditions in deep water, the statistical distribution of the wave surface elevation appears to be Gaussian. However, wind-generated waves exhibit inherent nonlinearities, evident in the form of sharper crests and more rounded, shallow troughs. As a result, nonlinear wave theories were developed to address these types of conditions. Most such theories dealt only with deterministic waves; however, one predominant random nonlinear wave theory has been studied extensively. Commonly known as second-order random wave theory, it is based on a Stokes perturbation expansion solution of the governing equations and the Fourier-Stieltjes spectral representation theorem for random processes. It has been presented by Tick (1959) and more recently studied by, among others, Kareem and Hsieh (1991) and Kareem et al. (1994, 1996). Here, the non-Gaussian wave kinematics are based on this theory, which is elaborated on in greater detail in the aforementioned papers and their references. A brief description

[1]Prof., Dept. of Civ. Engrg. and Geol. Sci., NatHaz Modeling Lab., 163 Fitzpatrick Hall, Univ. of Notre Dame, Notre Dame, IN 46556-0767.
[2]Formerly, Grad. Res. Asst., Univ. of Houston, Houston, TX 77204-4791.
[3]Doctoral Candidate, Dept. of Civ. Engrg. and Geol. Sci., 156 Fitzpatrick Hall, Univ. of Notre Dame, Notre Dame, IN.

Note. Associate Editor: Ross B. Corotis. Discussion open until November 1, 1998. To extend the closing date one month, a written request must be filed with the ASCE Manager of Journals. The manuscript for this paper was submitted for review and possible publication on November 11, 1996. This paper is part of the ***Journal of Engineering Mechanics***, Vol. 124, No. 6, June, 1998. ©ASCE, ISSN 0733-9399/98/0006-0668–0683/$8.00 + $.50 per page. Paper No. 14583.

of the approach by which these kinematics are cast in forms fit for analysis in the present framework is given in Appendix I.

According to the Morison equation, the wave force per unit length on a cylinder is composed of drag and inertia forces according to

$$f(x, z, t) = K_d V(x, z, t)|V(x, z, t)| + K_m A(x, z, t) \quad (1)$$

where $V(x, z, t)$ and $A(x, z, t)$ = non-Gaussian water-particle velocity and acceleration, respectively. The hydrodynamic coefficients K_d and K_m are given by $K_d = 0.5C_d\rho D$ and $K_m = C_m\rho V_D = (1 + C_a)\rho V_D = K_a + \rho V_D$, in which ρ is the fluid density; D and V_D are, respectively, the projected frontal area and the displaced volume of the member; C_d, C_m, and C_a, respectively, denote the drag coefficient, the inertia coefficient, and the added mass coefficient; and $K_a = C_a\rho V_D$. The coefficients C_d, C_m, and C_a are generally dependent on Reynolds number and Keulegan-Carpenter number, which will be assumed constant along the water depth.

To develop the power spectral density (PSD) of the force, we must first compute its cross-correlation. Let f_i denote the wave force at (x_i, z_i, t_i). Direct evaluation of the cross-correlation of wave forces acting at two locations $E[f_1 f_2]$, where $E[\cdot]$ is the expectation operator, becomes prohibitively complicated as it requires information on the joint probability density function of the fluid kinematics, which is non-Gaussian. Nonetheless, the evaluation will be carried out here by using Taylor series expansion and Price's theorem for Gaussian processes (Price 1958; Papoulis 1965; Borgman 1967). Thus, we express the non-Gaussian water-particle kinematics in terms of Gaussian processes as $V(x, z, t) = \sigma_V(z)W(U_V)$ and $A(x, z, t) = \sigma_A(z)Y(U_A)$, using a functional transformation (Grigoriu 1995; Winterstein 1985)

$$W(U_V) = U_V(x, z, t) + \alpha_{\tilde{V}}(z)[U_V^2(x, z, t) - 1] \quad (2a)$$

$$Y(U_A) = U_A(x, z, t)\{1 + \alpha_{\tilde{A}}(z)[U_A^2(x, z, t) - 3]\} \quad (2b)$$

where $U_V(x, z, t)$ and $U_A(x, z, t)$ = standardized forms of the first-order water-particle velocity and acceleration, respectively; σ_V and σ_A = standard deviations of the water-particle velocity and acceleration, respectively; $\alpha_{\tilde{V}}(z)$ is related to the skewness of the water-particle velocity; and $\alpha_{\tilde{A}}(z)$ is related to the kurtosis of the water-particle acceleration (see Appendix I). We have assumed here that the kurtosis of water-particle velocity is negligible to facilitate computations; however, because the skewness of water-particle acceleration is zero, we must retain its kurtosis so that the functional transformation in (2) does not revert to a Gaussian representation. Then, the cross-correlation is

$$E[f_1 f_2] = K_d^2\sigma_V^2(z_1)\sigma_V^2(z_2)E[W_1W_2|W_1W_2|] + K_dK_m\sigma_V^2(z_1)\sigma_A(z_2)E[W_1|W_1|Y_2] + K_mK_d\sigma_A(z_1)\sigma_V^2(z_2)E[W_2|W_2|Y_1] + K_m^2\sigma_A(z_1)\sigma_A(z_2)E[Y_1Y_2] \quad (3)$$

where the subscripts of W_i and Y_i $(i = 1, 2)$ identify their location (x_i, z_i, t_i). For convenience, let $G_1(\gamma_{VV})$ be defined as

$$G_1(\gamma_{VV}) = E[W_1W_2|W_1W_2|] = E[h(W_1)h(W_2)] \quad (4)$$

where γ_{VV} = covariance between $U_V(x_1, z_1, t_1)$ and $U_V(x_2, z_2, t_2)$; and $h(W) = W|W| \cdot G_1(\gamma_{VV})$ is a function of γ_{VV}; therefore, it can be expanded in a Taylor series at $\gamma_{VV} = 0$. By invoking Price's theorem to evaluate the various derivatives of $G_1(\gamma_{VV})$, it can be approximated up to γ_{VV}^3 as

$$G_1(\gamma_{VV}) = \frac{8\alpha_{\tilde{V}}(z_1)\alpha_{\tilde{V}}(z_2)}{\pi} + \frac{8}{\pi}\left\{1 + \frac{1}{2}[\alpha_{\tilde{V}}^2(z_1) + \alpha_{\tilde{V}}^2(z_2)]\right\}\gamma_{VV} + \frac{200}{2!\pi}\alpha_{\tilde{V}}(z_1)\alpha_{\tilde{V}}(z_2)\gamma_{VV}^2 + \frac{8}{3!\pi}\left\{1 - \frac{1}{2}[\alpha_{\tilde{V}}^2(z_1) + \alpha_{\tilde{V}}^2(z_2)]\right\}\gamma_{VV}^3 \quad (5)$$

Similarly, the remaining expectation terms in (3) are, respectively

$$G_2(\gamma_{VA}) = \sqrt{8/\pi}\left\{\left[1 + \frac{1}{2}\alpha_{\tilde{V}}^2(z_1)\right]\gamma_{VA} + \alpha_{\tilde{A}}(z_2)\gamma_{VA}^3\right\} \quad (6)$$

$$G_3(\gamma_{AV}) = \sqrt{8/\pi}\left\{\left[1 + \frac{1}{2}\alpha_{\tilde{V}}^2(z_2)\right]\gamma_{AV} + \alpha_{\tilde{A}}(z_1)\gamma_{AV}^3\right\} \quad (7)$$

with $\gamma_{VA} = \text{Cov}[U_V(x_1, z_1, t_1), U_A(x_2, z_2, t_2)]$, $\gamma_{AV} = \text{Cov}[U_A(x_1, z_1, t_1), U_V(x_2, z_2, t_2)]$. The last expectation term in (3) can be determined using a direct integration scheme as

$$G_4(\gamma_{AA}) = \gamma_{AA} + 6\alpha_{\tilde{A}}(z_1)\alpha_{\tilde{A}}(z_2)\gamma_{AA}^3 \quad (8)$$

where $\gamma_{AA} = \text{Cov}[U_A(x_1, z_1, t_1), U_A(x_2, z_2, t_2)]$. As a result, (3) can be rewritten as

$$E[f_1 f_2] = K_d^2\sigma_V^2(z_1)\sigma_V^2(z_2)G_1(\gamma_{VV}) + K_dK_m\sigma_V^2(z_1)\sigma_A(z_2)G_2(\gamma_{VA}) + K_mK_d\sigma_A(z_1)\sigma_V^2(z_2)G_3(\gamma_{AV}) + K_m^2\sigma_A(z_1)\sigma_A(z_2)G_4(\gamma_{AA}) \quad (9)$$

DYNAMIC WAVE LOAD EFFECTS

The jacket-type platform here is idealized by a candelabra configuration in which a rigid deck is supported by an assemblage of identical supporting cylindrical legs, which extend vertically from the seabed up through the water surface to its underside, as illustrated in Figs. 1(a–b). The choice of this configuration is made because wave forces acting on a vertical segment of an offshore tower may differ from those evaluated customarily using line structures. The platform spatial configuration governs the overall loading. Although for survivability considerations, the line structure approximation holds because the design waves have very long wavelengths; this may not be the case for other design considerations, e.g., fatigue, because seas characterized by relatively shorter wavelengths assume greater importance. Thus, this model is adopted to describe deck motion and its sensitivity to leg configuration. The governing equation of the deck motion is given by

$$m\ddot{X}_D(t) + c\dot{X}_D(t) + kX_D(t) = \tilde{F}(t) \quad (10)$$

where X_D = horizontal displacement of the deck in the direction of wave propagation; m, c, k, and $\tilde{F}(t)$ = generalized mass, viscous damping, and stiffness of and wave forces on the structural system, respectively. The mode shape $g(z) = 1/2(1 - \cos\{[\pi(z + d)]/L\})$ satisfies necessary platform boundary conditions, where d denotes the water depth and L is the height of the platform measured from the seabed up to the underside of the deck. Consequently, the horizontal displacement of the legs $y(z, t) = g(z)X_D(t)$.

The hydrodynamic force per unit length on the cylindrical platform legs is described by the relative motion form of the Morison equation (Chakrabarti 1987)

$$\tilde{f}(x, z, t) = K_d(V - \dot{y})|V - \dot{y}| + K_mA - K_a\ddot{y} \quad (11)$$

where the arguments of the variables have been omitted for brevity. It should be further noted that for a particular leg, the horizontal coordinate x is considered fixed. For $\dot{y} << V$, the terms of order $\dot{y}^2$ or higher are negligible and (11) may be approximated by replacing the drag term with a truncated Taylor series about $\dot{y} = 0$ as follows:

$$\tilde{f}(x, z, t) = K_d[V|V| - 2|V|\dot{y}] + K_mA - K_a\ddot{y} \quad (12)$$

Subsequently, the generalized wave force on the deck defined in (10) can be given explicitly by

$$\tilde{F}(t) = \sum_{n=1}^{N}\int_{L_f}\tilde{f}(x_n, z, t)g(z)\,dz \quad (13)$$

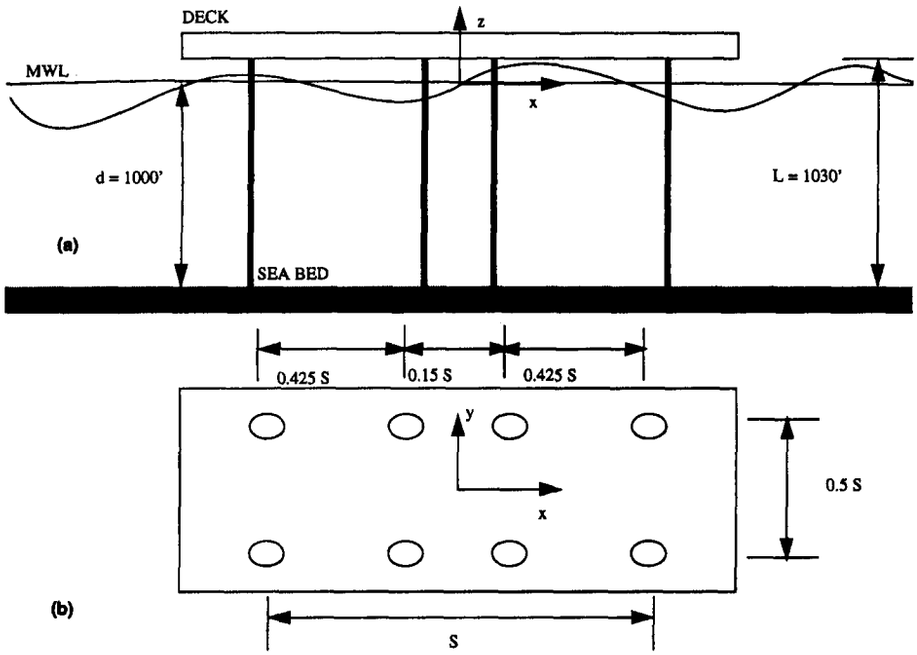

FIG. 1. Schematic of Model Jacket-Type Structure: (a) Side View; (b) Top View

where N indicates the number of platform legs; the subscript n identifies the wave force on the nth leg; and L_f denotes the integration range in which wave force is considered effective. Substituting $\tilde{F}(t)$ into (10) and rearranging leads to

$$m_e\ddot{X}_D(t) + c_e\dot{X}_D(t) + kX_D(t) = F(t) \tag{14}$$

where

$$m_e = m + N\int_{L_f} K_a g^2(z)\,dz, \quad c_e = c + c_h$$

with

$$c_h = \sum_{n=1}^{N}\int_{L_f} 2K_d\{|V|\}_{x=x_n} g^2(z)\,dz$$

and

$$F(t) = \sum_{n=1}^{N}\int_{L_f}\{K_d|V|V + K_m A\}_{x=x_n} g(z)\,dz$$

Note from the foregoing expressions that additional damping results from the relative motion of legs with respect to the fluid, which aids in reducing the platform response. Employing the closure approximation that water-particle velocity and deck velocity are uncorrelated (e.g., Sigbjornsson and Morch 1982), the averaged dissipated energy per unit time due to c_h may be related to an equivalent damping coefficient, namely, (Kareem and Hsieh 1991)

$$E[c_h\dot{X}_D^2] = E[c_h]E[\dot{X}_D^2] = c_{eq}E[\dot{X}_D^2] \tag{15}$$

$$c_{eq} = \sqrt{8/\pi}NK_d\int_{L_f}\left\{1 + \frac{1}{2}\alpha_{\dot{V}}^2(z)\right\}\sigma_V(z)g^2(z)\,dz \tag{16}$$

Hereafter, we will use c_{eq} to quantify hydrodynamic damping. This procedure removes time dependency from the damping coefficient.

GENERALIZED FORCE AND RESPONSE SPECTRA

The evaluation of the integral wave force on a jacket-type platform is complicated by the fact that the platform-submerged area fluctuates in time. The intermittent wave forces on a jacket-type platform introduced by taking into consideration the instantaneous wave surface elevation are regarded as second-order wave forces. This is in addition to second-order contributions of wave forces that result from wave-wave interactions. The present study is directed primarily toward quantifying the effects of the nonlinear, non-Gaussian water-particle kinematics on the wave forces and platform response. The contributions of the force above the mean water level also can be included in the analysis with the addition of sizeable computational complexity, which is a subject of a current investigation. Hence, instead of extending the wave kinematics up to the free surface, the generalized wave loading described in (14) is evaluated by integrating wave forces only from the seabed up to the mean water level, namely

$$F(t) = \sum_{n=1}^{N}\int_{-d}^{0} f_n(z, t)g(z)\,dz \tag{17}$$

where $f_n(z, t)$ represents $\{K_d|V|V + K_m A\}_{x=x_n}$. Accordingly, the mean and autocorrelation function of the generalized force $F(t)$ are

$$E[F(t)] = \sqrt{8/\pi}NK_d\int_{-d}^{0}\alpha_{\dot{V}}(z)\sigma_V^2(z)g(z)\,dz \tag{18}$$

and

$$R_{FF}(\tau) = \sum_{i=1}^{N}\sum_{j=1}^{N}\int_{-d}^{0}\int_{-d}^{0}\frac{1}{2}[R_{f_if_j}(z, z', \tau) + R_{f_if_j}(z', z, \tau)]g(z)g(z')\,dz\,dz' \tag{19}$$

where $R_{f_if_j}(z', z, \tau) = E[f_i(z', t)f_j(z, t + \tau)]$. Substituting the autocorrelation function of wave forces from (9) into (19) and simplifying, the autocorrelation function of the generalized force becomes

$$R_{FF}(\tau) = \sum_{i=1}^{N}\sum_{j=1}^{N}\int_{-d}^{0}\int_{-d}^{0}\{K_d^2\sigma_V^2(z)\sigma_V^2(z')G_1(\gamma_{VV}) + K_m^2\sigma_A(z)\sigma_A(z')G_4(\gamma_{AA})\}g(z)g(z')\,dz\,dz' \tag{20}$$

where it should be recalled that γ_{VV} and γ_{AA} are functions of

spatial location and τ, though the arguments have been omitted for brevity. It can be shown (Kareem and Hsieh 1991) that the cross-terms involving γ_{VA} and γ_{AV} cancel. The corresponding PSD is given by

$$S_{FF}(f) = \delta(f)N^2 \int_{-d}^{0}\int_{-d}^{0} P_1(z, z')g(z)g(z')\,dz\,dz' + \sum_{i=1}^{N}\sum_{j=1}^{N}\int_{-d}^{0}\int_{-d}^{0}\{P_2(x_i, z, x_j, z', f) + P_3(x_i, z, x_j, z', f)\}g(z)g(z')\,dz\,dz' \quad (21)$$

where

$$P_1 = \frac{8}{\pi} K_d^2 \alpha_{\hat{V}}(z)\alpha_{\hat{V}}(z')\sigma_{\hat{V}}^2(z)\sigma_{\hat{V}}^2(z') \quad (22)$$

$$P_2(x_i, z, x_j, z', f) = K_d^2\sigma_{\hat{V}}^2(z)\sigma_{\hat{V}}^2(z')\left\{\frac{8}{\pi}\left[\frac{2 + \alpha_{\hat{V}}^2(z) + \alpha_{\hat{V}}^2(z')}{2}\right]\hat{S}_{VV}(x_i, z, x_j, z', f) + \frac{100}{\pi}\alpha_{\hat{V}}(z)\alpha_{\hat{V}}(z')\hat{S}_{VV}^{*2}(x_i, z, x_j, z', f) + \frac{2}{3\pi}[2 - \alpha_{\hat{V}}^2(z) - \alpha_{\hat{V}}^2(z')]\hat{S}_{VV}^{*3}(x_i, z, x_j, z', f)\right\} \quad (23)$$

and

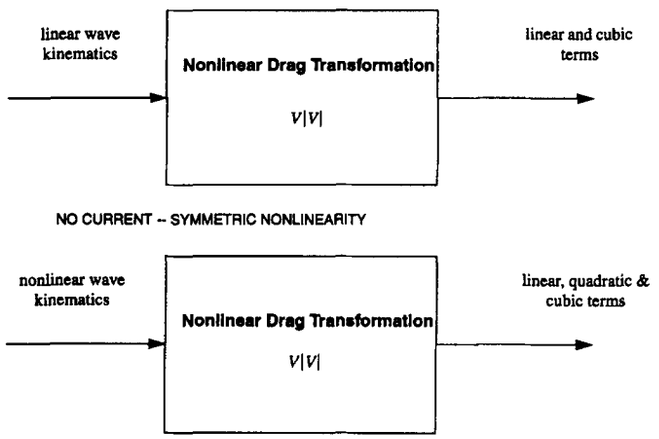

FIG. 2. Schematic of Drag Transformation for Linear/Nonlinear Waves

$$P_3(x_i, z, x_j, z', f) = K_m^2\sigma_A(z)\sigma_A(z')\{\hat{S}_{AA}(x_i, z, x_j, z', f) + 6\alpha_{\hat{A}}(z)\alpha_{\hat{A}}(z')\hat{S}_{AA}^{*3}(x_i, z, x_j, z', f)\} \quad (24)$$

where the superscripts *2 and *3 = second- and third-fold convolutions of the standardized PSD, respectively. The standardized PSDs of the water-particle kinematics are given as follows:

$$\hat{S}_{VV}(x_i, z, x_j, z', f) = S_{V^{(1)}V^{(1)}}(x_i, z, x_j, z', f)/[\sigma_{V^{(1)}}(z)\sigma_{V^{(1)}}(z')] \quad (25a)$$

$$\hat{S}_{AA}(x_i, z, x_j, z', f) = S_{A^{(1)}A^{(1)}}(x_i, z, x_j, z', f)/[\sigma_{A^{(1)}}(z)\sigma_{A^{(1)}}(z')] \quad (25b)$$

where $S_{V^{(1)}V^{(1)}}(x_i, z, x_j, z', f)$ and $S_{A^{(1)}A^{(1)}}(x_i, z, x_j, z', f)$ = the power spectral densities of the water-particle velocity and acceleration based on linear wave theory, respectively (Kareem et al. 1994). If $\alpha_{\hat{V}}(z)$ and $\alpha_{\hat{A}}(z)$ are considered negligible, the PSD of the generalized force reduces exactly to that of Borgman (1965) for linear waves, which contains only linear and third-order terms. A schematic of the nonlinear drag transformation is shown in Fig. 2. The figure indicates that for linear waves, the nonlinear drag term is statistically symmetric (odd-order central moments are zero); therefore, the nonlinearity could be approximated appropriately by a sum of linear and cubic terms (e.g., Tognarelli et al. 1997) but is not quadratic in nature. If a nonzero current had been assumed, the nonlinearity would be asymmetric and quadratic terms also would be present for linear wave input (Spanos and Donley 1990; Kareem and Zhao 1994; Kareem et al. 1995; Tognarelli et al. 1997). For a compliant structure like a tension-leg platform, if the platform displaced position is taken into consideration in the force expression, a quadratic term also will be admitted even though the form of the nonlinearity remains symmetric (Li and Kareem 1992). On the other hand, when the waves are nonlinear, a quadratic interaction also is introduced because of the nature of the higher-order terms in the kinematic expressions themselves [see (23)].

In this study, the primary interest is the standard deviation of the deck displacement of a jacket-type platform for several leg spacing configurations in a nonlinear random wave field. Having the mean and power spectrum of the generalized force, second-order response statistics can be acquired via random vibration analysis.

NUMERICAL RESULTS AND ANALYSIS

An idealized jacket-type platform situated in water of 304.8 m (1,000 ft) depth [Fig. 1(a)] is used to demonstrate the meth-

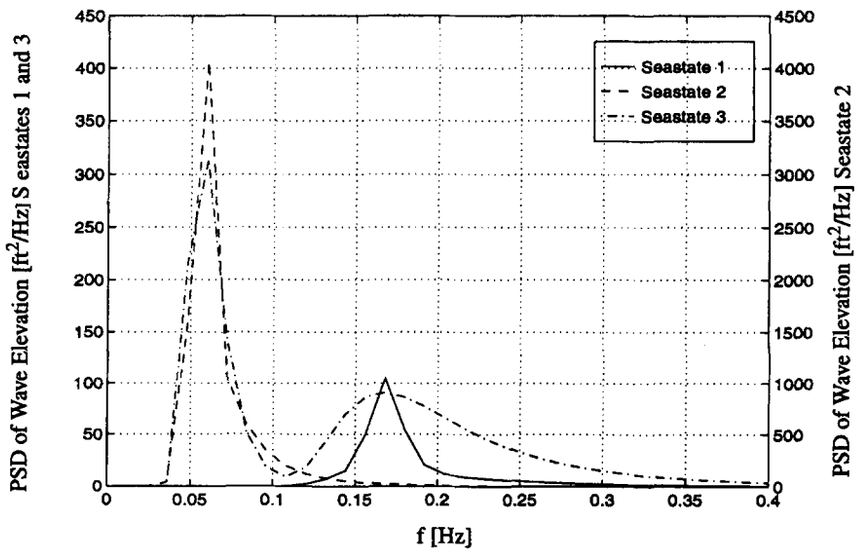

FIG. 3. Linear Wave Elevation PSDs Used in Examples

odology presented here. The dimensions of the platform and the leg configuration are illustrated in the top view given by Fig. 1(b), where S denotes primary leg spacing, which will be used as a parameter and nondimensionalized by a reference length in the numerical results of the random response of the deck. The reference length is $S_n = \pi g/\omega_n^2$, where ω_n denotes the natural frequency of the platform system in rad/s and g = 9.81 m/s^2 (32.2 ft/s^2). Thus, S_n is half the wavelength of a monochromatic wave train in deep water with frequency equal to the natural frequency of the platform system. The platform considered has eight cylindrical legs each 313.94 m (1,030 ft) long and 0.50 m (1.64 ft) in diameter. For the sake of illustration, the inertia and drag coefficients C_m and C_d of the legs are chosen to be 1.7 and 1.0, respectively. The weight of the effective mass m_e of the platform system is 17,792.8 kN (4,000 kips); the stiffness of the platform system is such that the system natural frequency is 0.167 Hz [so, for this platform, S_n = 28.0 m (91.9 ft)] and the viscous damping ratio of the platform system is 5%. In addition, the hydrodynamic damping based on (16) is included in the numerical computations. Three dis-

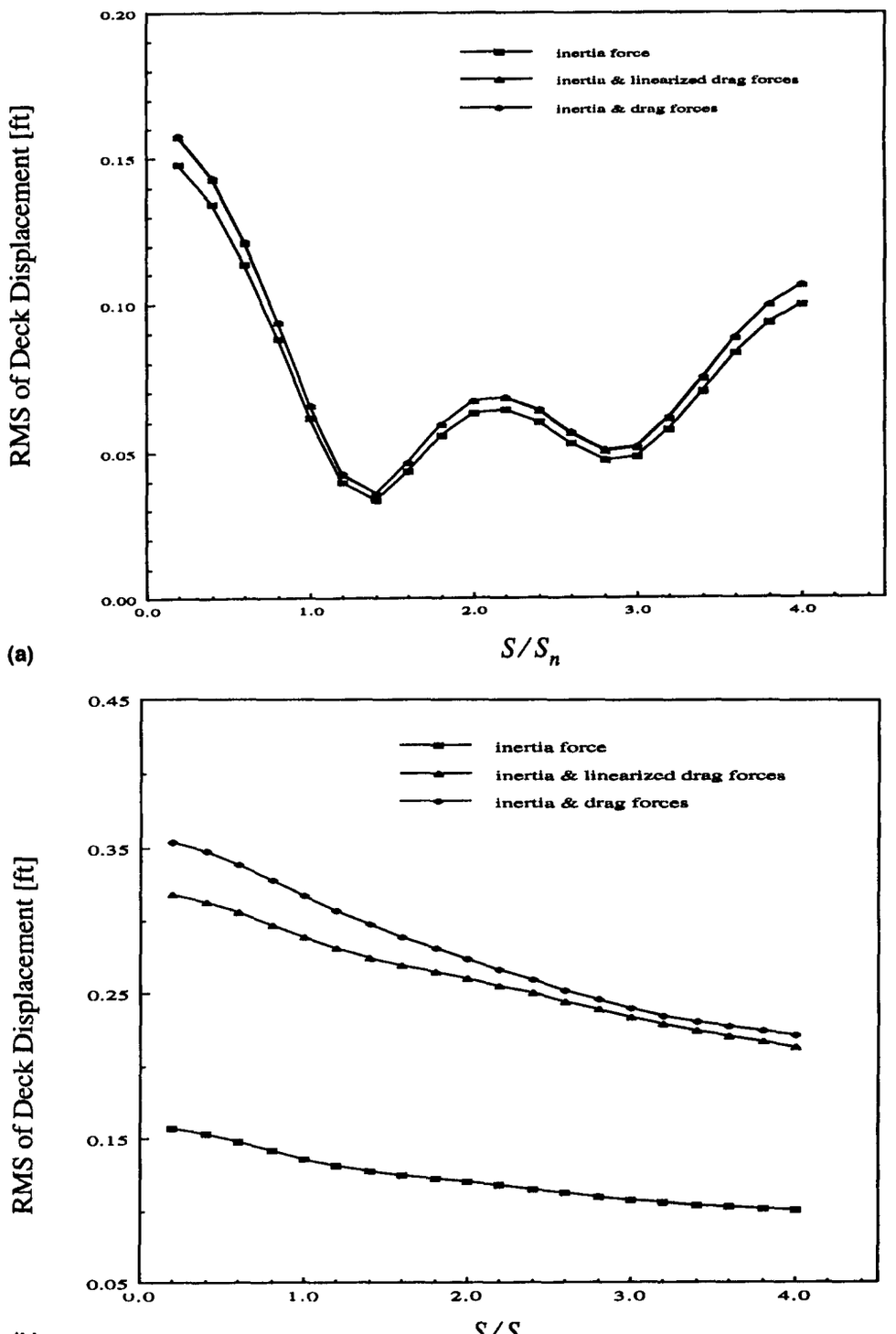

FIG. 4. (a) RMS Deck Displacement (Linear Waves, Sea State 1); (b) RMS Deck Displacement (Linear Waves, Sea State 2); (c) RMS Deck Displacement (Linear Waves, Sea State 3)

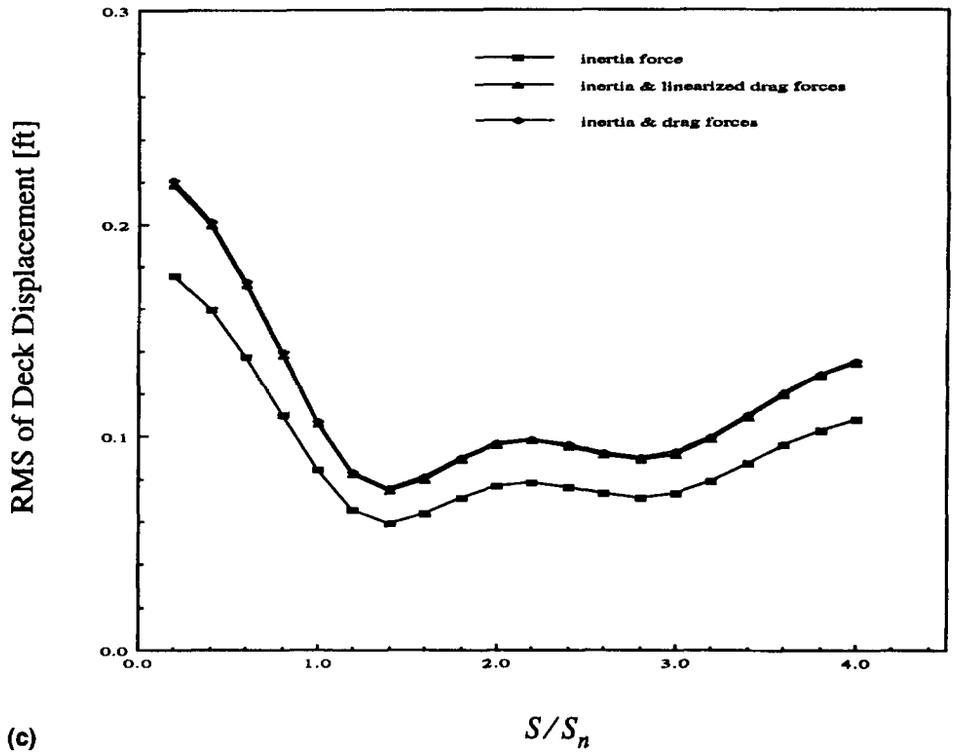

(c)

FIG. 4. (*Continued*)

tinct sea states are considered (Fig. 3). The first is characterized by a JONSWAP spectrum with peak wave frequency of 0.167 Hz and peakedness of 7.24 [H_s = 2.39 m (7.84 ft)]; the second also is characterized by a JONSWAP spectrum with peak wave frequency of 0.0557 Hz and peakedness of 3.78 [H_s = 12.12 m (39.77 ft)]; the third is characterized by an Ochi-Hubble six-parameter spectrum with peak wave frequencies of 0.0557 Hz and 0.167 Hz, significant wave heights of 3.66 m (12 ft) and 3.96 m (13 ft), and shape factors of 2.0 and 1.0 (Chakrabarti 1987). Although the first two sea states are typical representations of locally wind-generated waves only, the third additionally incorporates the effects of low-frequency swell.

Results Based on Linear Wave Theory

Deck displacement statistics for three sea states, based on linear wave theory, are presented in Figs. 4(a–c). Illustrated in Fig. 4(a) is the variation of the RMS of the deck displacement with respect to the leg spacing ratio (LSR) S/S_n in sea state 1, for analyses considering the inertia force alone, the inertia force combined with linearized drag force, and the inertia force combined with nonlinear drag force. To obtain the linearized drag force spectrum for linear waves from the generalized force spectrum given in (21)–(24), $\alpha_{\dot{V}} = \alpha_{\dot{A}} = 0$, by virtue of the linear waves, and the remaining higher-order convolution terms are neglected in the computations to linearize the force expression itself. Note that the response is caused by predominantly the inertia force because the combined forces give rise to a small increase in the response level. However, it should be noted that the response level of the deck changes significantly with respect to the LSR; it attains relatively lower values at LSRs ranging from approximately 1.0 to 3.5 and relatively higher values at other LSRs. This variation can be attributed to the wave phase effects, under the influence of which, at LSRs of very small values, all legs experience nearly the same wave force from the dominant wave of 0.167 Hz at the same instant; otherwise, legs are subjected to the wave force, at different phases, from the dominant wave. Local maxima at LSRs of 2.0 and 4.0 correspond to the case where inputs at the dominant wave frequency are in phase on two and four pairs of platform legs, respectively. Similarly, Fig. 4(b) indicates the variation of the RMS of the deck displacement with respect to the LSR in sea state 2. This figure shows that the drag force induces a response that is twice as large as that induced by the inertia force, and linearization leads to underestimation of the response level by 3–9%, depending on the LSR. Unlike the case of sea state 1, the RMS of the deck displacement in sea state 2 decreases monotonically with the LSR, which can be attributed to the fact that the dominant wave of 0.0557 Hz has a relatively long wavelength such that for leg configurations of interest, wave forces on legs cancel each other gradually in accordance with the LSR. Fig. 4(c) shows the variation of the RMS of the deck displacement in sea state 3. These response patterns are similar to those observed in sea state 1, indicating that the forces caused by waves having a spectral peak of 0.167 Hz are relatively dominant over those for waves having a spectral peak of 0.0557 Hz and thus the inertia force dominates over the drag force. Indeed, the inertia force is responsible for nearly 80% of the displacement level of the deck. In obtaining these response statistics, the hydrodynamic damping ratios, which are 0.48, 4.75, and 1.75%, respectively, in sea states 1, 2, and 3, have been included in the analysis. Overall, as seen in Figs. 4(a–c), the displacement level of the deck varies significantly with respect to LSR, suggesting that the wave phase difference indeed can be used to minimize the motion of a jacket-type platform in random waves, a fact noted by naval architects for deterministic waves. Furthermore, the linearization of the drag force has been shown to result in a nonconservative estimate of the deck displacement and thus may have implications concerning the fatigue life prediction of a platform.

Fig. 5 illustrates the PSD of the deck displacement for an LSR of 2.0 in sea state 2. When nonlinearity of the drag force is included, the PSD has a nonzero value at zero and low frequencies and an enhanced secondary peak near the natural frequency of the platform. Even for linear waves, the nonlinear

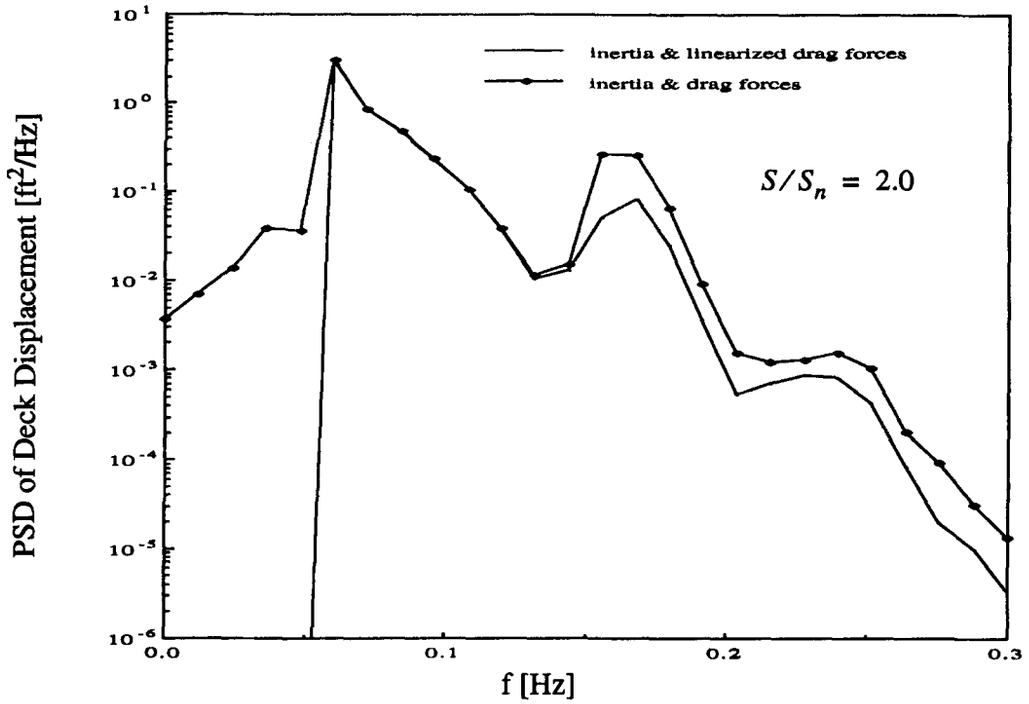

FIG. 5. PSD of Deck Displacement (Linear Waves, Sea State 2)

TABLE 1. Wave Cancellation/Amplification Effects

LSR = 4.0; S = 110.3 m (367.5 ft)			LSR = 2.0; S = 55.13 m (183.8 ft)		
f (Hz) (1)	λ (m/ft) (2)	I/O (3)	f (Hz) (4)	λ (m/ft) (5)	I/O (6)
0.0835	220.5 (735.0)	O	0.1181	110.3 (367.5)	O
0.1181	110.3 (367.5)	I	0.1670	55.13 (183.8)	I
0.1446	73.50 (245.0)	O	0.2045	36.75 (122.5)	O
0.1670	55.13 (183.8)	I	0.2362	27.56 (91.88)	I
0.1867	44.10 (147.0)	O	0.2641	22.05 (73.50)	O
0.2045	36.75 (122.5)	I	0.2893	18.38 (61.25)	I
0.2209	31.50 (105.0)	O	0.3124	15.75 (52.50)	O
0.2362	27.56 (91.88)	I	0.3340	13.78 (45.94)	I
0.2505	24.50 (81.67)	O	0.3543	12.25 (40.83)	O
0.2641	22.05 (73.50)	I	0.3734	11.03 (36.75)	I
0.2769	20.05 (66.82)	O	0.3917	10.02 (33.41)	O
0.2893	18.38 (61.25)	I	0.4091	9.188 (30.63)	I
0.3011	16.96 (56.54)	O	0.4258	8.481 (28.27)	O
0.3124	15.75 (52.50)	I	0.4418	7.875 (26.25)	I
0.3234	14.90 (49.00)	O	0.4574	7.350 (24.50)	O
0.3340	13.78 (45.93)	I	0.4724	6.891 (22.97)	I
0.3443	12.97 (43.24)	O	0.4869	6.485 (21.62)	O
0.3543	12.25 (40.83)	I	0.5010	6.125 (20.42)	I
0.3640	11.61 (38.68)	O	0.5147	5.803 (19.34)	O
0.3734	11.03 (36.75)	I	0.5281	5.513 (18.38)	I
0.3827	10.50 (35.00)	O	0.5412	5.250 (17.50)	O

drag transformation introduces spreading of the energy outside the frequency range of the input water-particle velocity spectrum, a phenomenon that is lost by linearization. Clearly, linearization of the drag force also may yield inaccurate estimates of such response statistics as RMS of the deck displacement and velocity, which are in turn likely to influence fatigue life estimates.

The cancellation/amplification effects, which introduce additional spectral peaks, are studied here by introducing variable leg spacing on the platform. This approach has been adopted over using a fixed spacing or merely a single column, as commonly reported in the literature, because the behavior of a section of an offshore structure consisting of several members can vary significantly based on its spatial layout and a basic multiple-legged structure, while maintaining simplicity, more closely approximates a practical platform section than does a single submerged column. Additional peaks in Fig. 5 and subsequent figures may be explained more clearly by referring to Table 1, which indicates frequencies at which inputs are in phase or out of phase at the front and rear legs of the model platform. The left side of the table pertains to the case where the LSR is 4.0 [(S = 108 m (367.5 ft)] and the right side pertains to the case where the LSR is 2.0 [(S = 54 m (183.8 ft)]. The table indicates frequency components in the input spectrum, which have wavelengths that correspond to $S/[(n + 1)/2]$, $n = 0, 1, \ldots, 20$. That is, for these input components, an integer number of cycles or an integer number plus one-half cycle is equal to the front-to-rear spacing for the platform configuration considered. In the former case, such an input is in phase (I) at the front and rear legs of the platform. In the latter case, the frequency component of the input is out of phase (O) at the front and rear legs of the platform. Referring to the right side of the table and Fig. 5, notice, for example, the spectral peak at 0.2362 Hz and the approach to a spectral trough at 0.3124 Hz due to phase considerations. The case of an LSR of 0.2 [(S = 5.4 m (18.38 ft)] has not been tabulated. This is because the legs are packed so tightly that, for the long input wavelengths considered in this study, minimal cancellation or amplification caused by wave phase effects is observed.

Results Based on Nonlinear Wave Theory

In the following discussion, the generalized wave force and the response of the platform deck based on a nonlinear wave theory are presented. For all of the following cases, a nonlinear form for the drag term also is employed. The second- and third-order dependence of the force spectrum for nonlinear waves on the kinematics' spectra [see (21)–(24)] introduces energy at sum and difference frequencies and spreading of the energy about the first-order peak wave frequency, increasing both the RMS of the force and response as well as their PSDs across the range of frequencies considered. Fig. 6(a) exhibits the relationship of the RMS of the generalized force on the deck to the LSR in sea state 1. Though hardly noticeable in

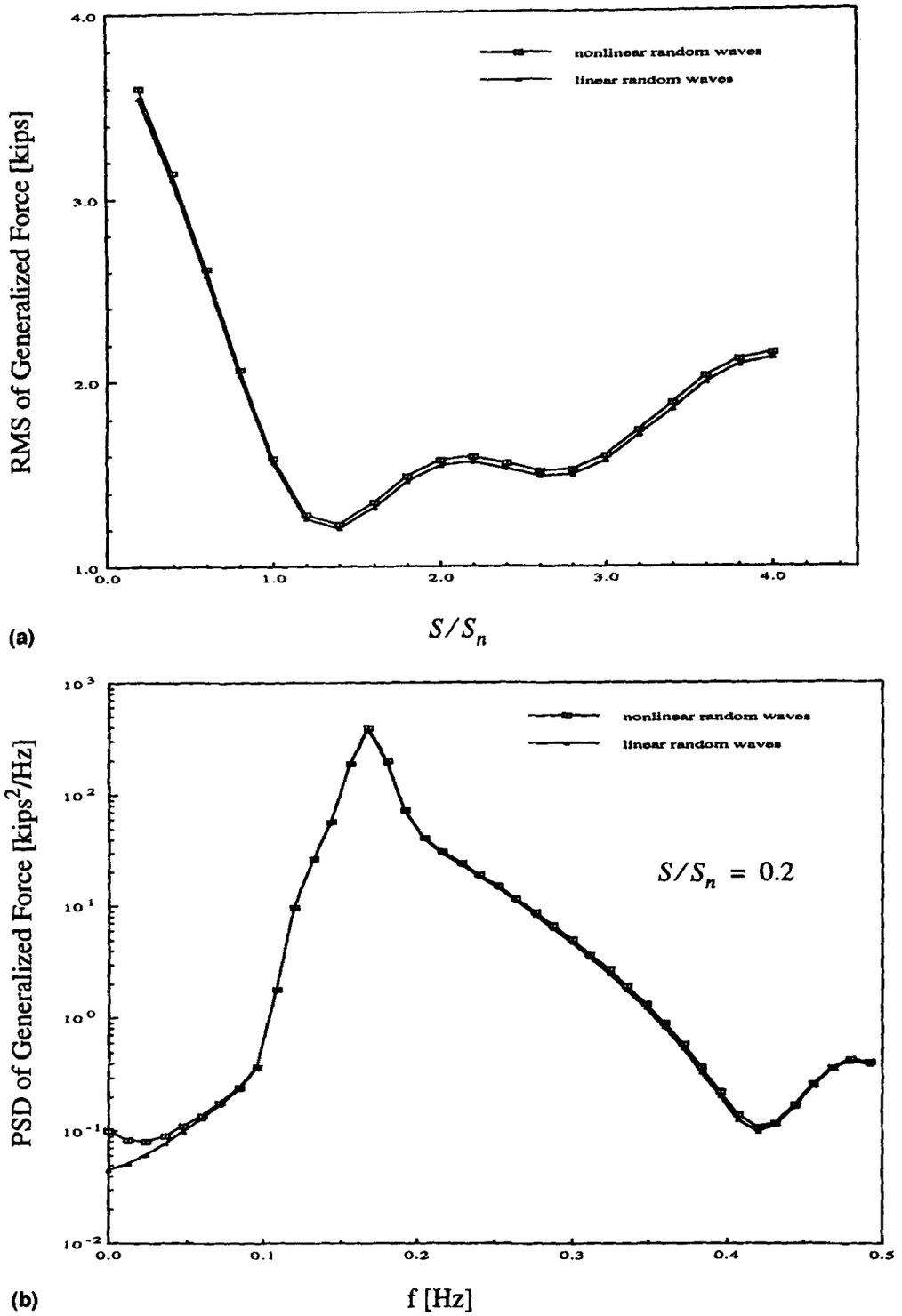

FIG. 6. (a) RMS Generalized Force (Sea State 1); (b) PSDs of Generalized Force (Sea State 1, LSR = 0.2); (c) PSDs of Generalized Force (Sea State 1, LSR = 2.0); (d) RMS Deck Displacement (Sea State 1)

the figure, model data indicates that the level of the generalized force is increased by the wave nonlinearity by 1.4–1.9%, depending on the LSR. Fig. 6(b) shows the PSD of the generalized forces on the deck for an LSR of 0.2 in sea state 1. The PSD is increased slightly because of wave nonlinearity, with an increase of 2.7% at the spectral peak of 0.167 Hz. No additional peaks are evident in the PSD because of wave cancellation caused by the tightness of the leg spacing for this case. Fig. 6(c) shows the PSD of the generalized forces on the deck for an LSR of 2.0 in sea state 1. From this, it is seen that because of wave nonlinearity the PSD increases by 2.6% near the spectral peak of 0.167 Hz and shows an overall slight increase over frequencies of interest. Moreover, by comparing results between Figs. 6(b and c), it is clear that the shape of the PSD of the generalized force on the deck is related to the leg configuration. Amplification and cancellation effects are evident in the additional peaks and troughs in Fig. 6(c) which may be related to in-phase and out-of-phase frequency components noted on the right side of Table 1. Fig. 6(d) shows the RMS of deck displacement as it varies with the LSR in

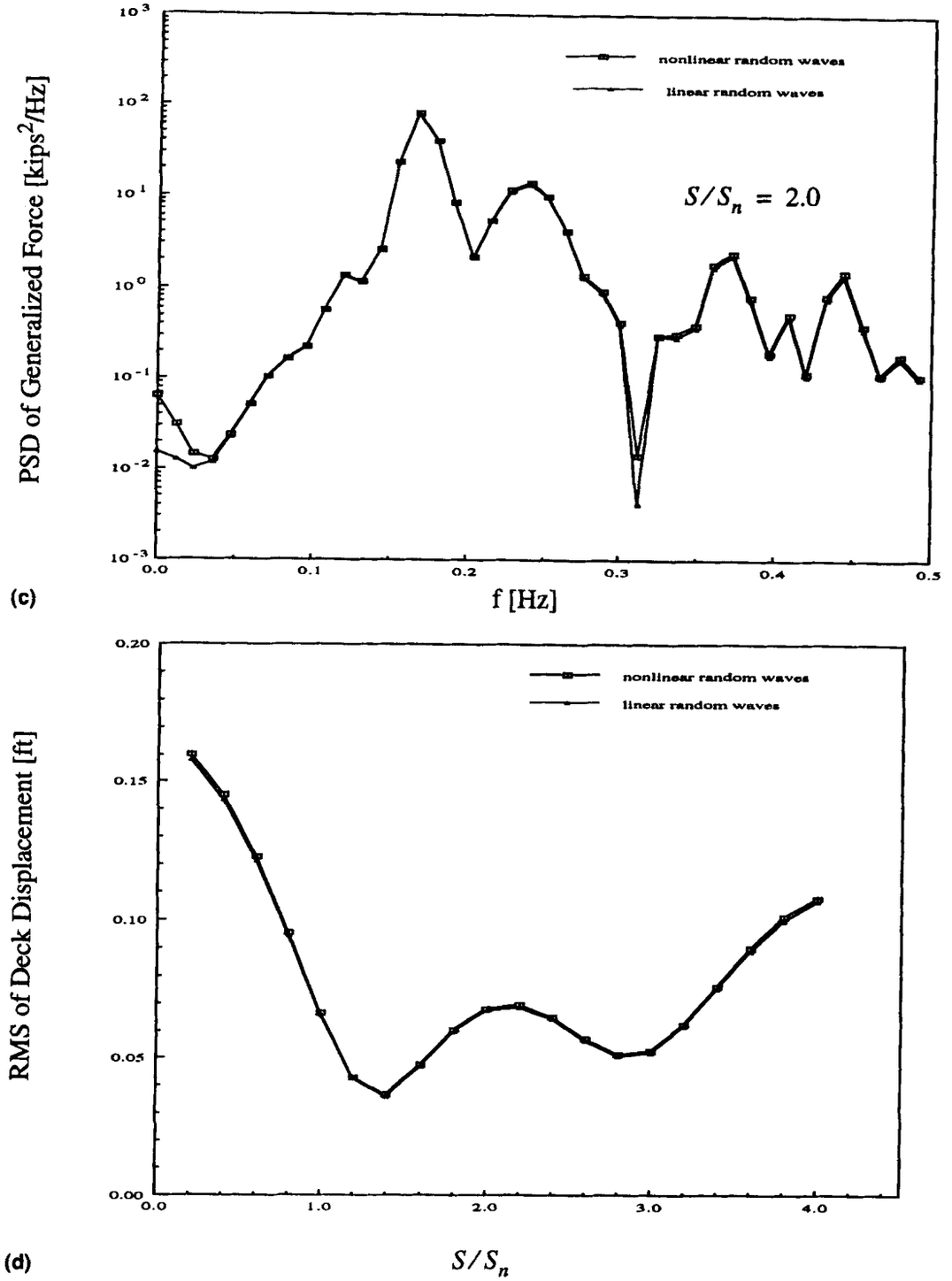

FIG. 6. (*Continued*)

sea state 1. This figure shows that the nonlinear result is 1.2–1.6% larger than the linear result depending on the LSR.

Fig. 7(a) shows the variation of the RMS of the generalized force on the deck with respect to the LSR in sea state 2. In this figure, the level of the generalized force on the deck is increased, because of wave nonlinearity, by approximately 1.5% for an LSR of 4.0 and up to 2.3% for an LSR of 0.2. Because of the large wavelength of the dominant wave, significant maxima and minima are not evident over the range of leg spacing considered. Fig. 7(b) illustrates the PSD of the generalized forces on the deck for an LSR of 0.2 in sea state 2 using linear and nonlinear waves, respectively. The figure indicates that the nonlinear result is generally higher than the linear one, as reflected by an increase of 2.1% at the spectral peak of 0.0557 Hz and an increase of 10% or more at frequencies higher than 0.167 Hz. Fig. 7(c) shows the PSD of the generalized forces on the deck for an LSR of 2.0 in sea state 2. This shows that an increase of 2.1% above the PSD based on the linear theory is induced near the spectral peak of 0.0557 Hz by the wave nonlinearities, and the PSD is, in general, increased, most significantly at higher frequencies. Comparison of the results between Figs. 7(b and c) shows that the effects of wave phase difference become clear at the larger LSR in terms of significantly reducing the value of the spectral

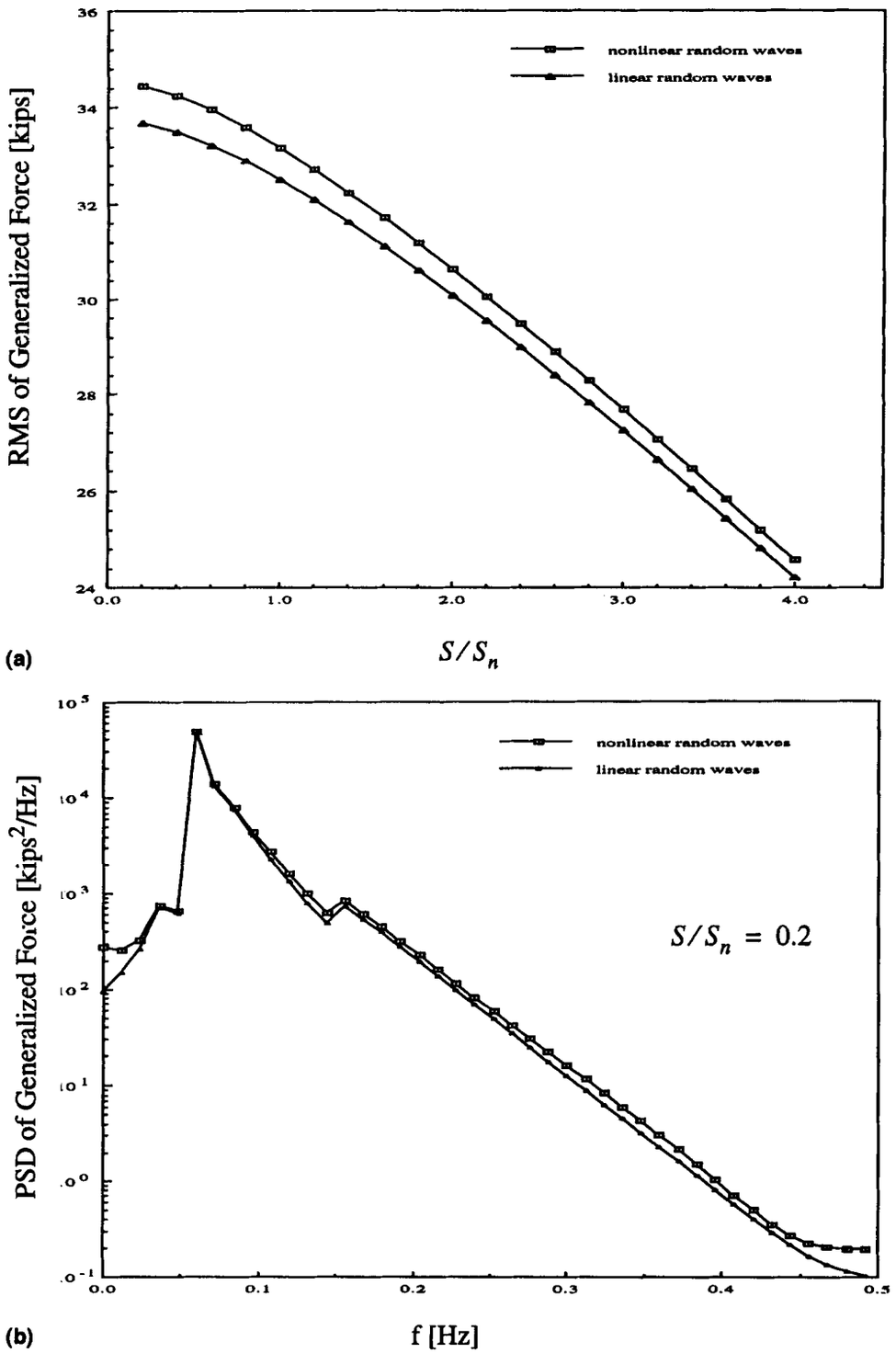

FIG. 7. (a) RMS Generalized Force (Sea State 2); (b) PSDs of Generalized Force (Sea State 2, LSR = 0.2); (c) PSDs of Generalized Force (Sea State 2, LSR = 2.0); (d) RMS Deck Displacement (Sea State 2)

peak in the neighborhood of the platform natural frequency, 0.167 Hz. The more pronounced nature of this peak in Fig. 7(c) as well as the surrounding troughs at 0.1181 and 0.2045 Hz and several peaks and troughs located in the range of higher frequencies are attributable to the leg spacing according to Table 1. Fig. 7(d) shows the relationship of the RMS of the deck displacement to the LSR in sea state 2. Here, note that the response based on nonlinear analysis is higher than those based on linear analysis for any leg configuration. The differences between the two estimates are 4.2 and 2.5% at LSRs of 0.2 and 4.0, respectively.

The dependence of the RMS of the generalized force on the deck on the LSR in sea state 3 is given in Fig. 8(a). Observe here that nonlinear wave analysis exhibits an increase in the RMS of the generalized force of 9.7% at LSR of 0.2. This increase diminishes to 6.1% at an LSR of 1.0 and then grows monotonically up to 8.4% at an LSR of 4.0. The overall trends in Fig. 8(a) appear to be a combination of those found in Figs.

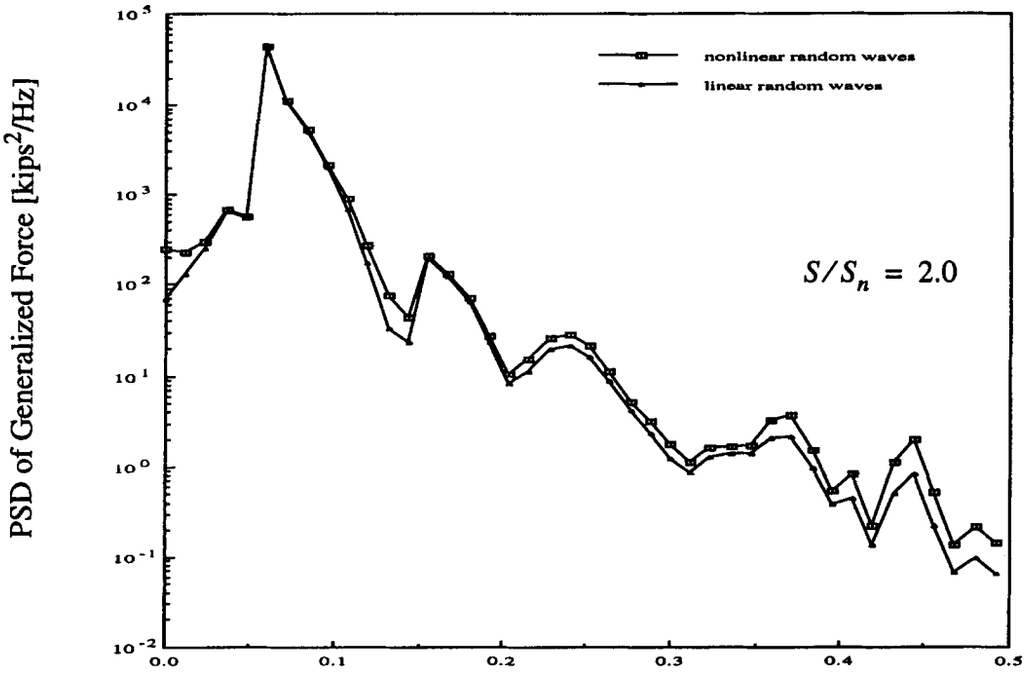

(c)

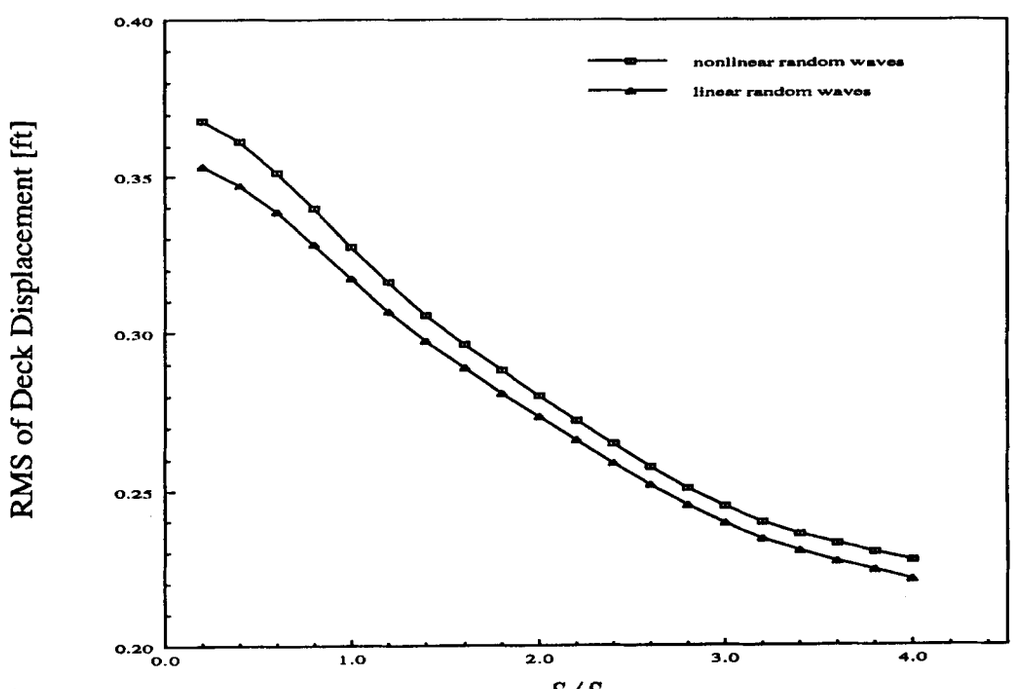

(d)

FIG. 7. (*Continued*)

6(a) and 7(a), which may be expected because the wave field is represented by a PSD with peaks at both 0.0557 and 0.167 Hz. Fig. 8(b) presents PSDs of the generalized force on the deck at an LSR of 0.2 in sea state 3. From the figure, it is noted that the nonlinear analysis admits larger PSD values relative to the linear analysis, with discrepancies of 4.7% at the spectral peak at 0.0557 Hz and 25.6% at the secondary spectral peak at 0.167 Hz. However, because of the tightness of the leg spacing no other spectral peaks are evident other than at the dominant wave frequencies because there are no significant cancellation or amplification effects. By comparison, Fig. 8(c) shows the PSD of the generalized forces on the deck at an LSR of 2.0 in sea state 3. Note here that because of the wave nonlinearities, the two spectral peaks, located at 0.167 and 0.236 Hz, are increased by 26.1 and 40.2%, respectively, and an increase of 4.4% occurs at the major spectral peak frequency of 0.0557 Hz. Further, Fig. 8(d) presents the PSD of the generalized forces on the deck at an LSR of 4.0 in sea state 3. As in the case presented for an LSR of 2.0, there is an overall increase in the PSD of the generalized force on the deck when the wave nonlinearities are included. Comparing Figs. 8(c) and (d) and referring to Table 1, note that because of differences in leg configuration, the positions and magnitudes of peaks in the PSDs of the generalized force on the

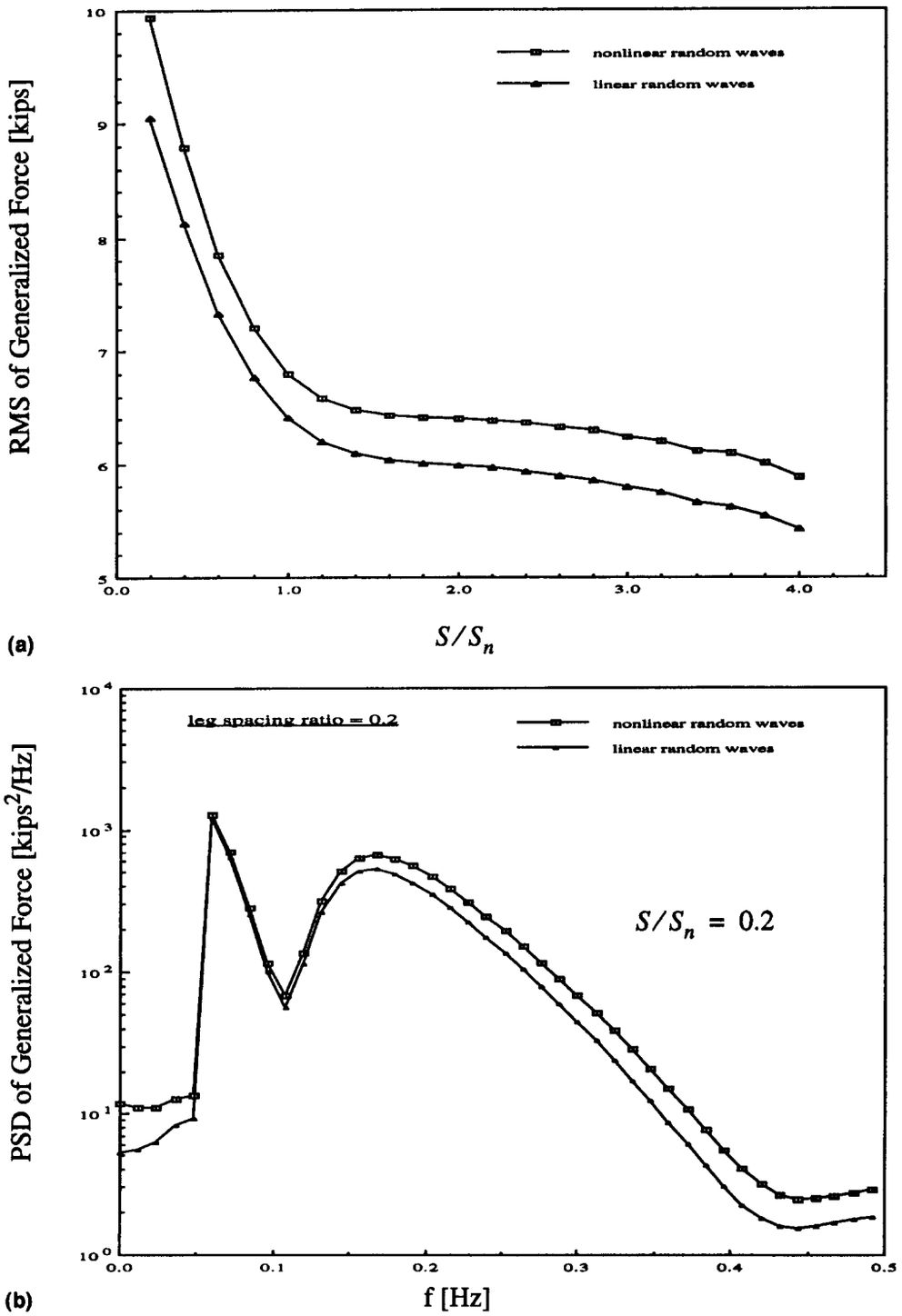

FIG. 8. (a) RMS Generalized Force (Sea State 3); (b) PSDs of Generalized Force (Sea State 3, LSR = 0.2); (c) PSDs of Generalized Force (Sea State 3, LSR = 2.0); (d) PSDs of Generalized Force (Sea State 3, LSR = 4.0); (e) RMS Deck Displacement (Sea State 3)

deck are distinct from each other. Note, for example, a peak in the PSD at 0.3124 Hz for an LSR of 4.0 and a trough at the same frequency for an LSR of 2.0, because, as indicated on Table 1, inputs at this frequency amplify one another in the former case but cancel one another in the latter case. In particular, the major spectral peak at 0.0557 Hz for an LSR of 2.0 is approximately 10% greater than that for an LSR of 4.0. Also, the secondary spectral peak at 0.167 Hz for an LSR of 2.0 is half as large as that for an LSR of 4.0, particularly because energy at this frequency is not only in phase at the front and rear legs of the platform for an LSR of 4.0, but also nearly in phase at the center legs as well because its wavelength is equal to half the leg spacing (see Table 1). These major differences, on the other hand, may account for the fact that the RMS of the generalized forces on the deck, corresponding to LSRs of 2.0 and 4.0, respectively, are approximately of the same order, as shown in Fig. 8(a). Although the RMS of the generalized forces on the deck are nearly the same, the response level of the deck at an LSR of 4.0 can be expected to be higher than that at an LSR of 2.0, considering that the natural frequency of the structure system is 0.167 Hz and the input energy at this frequency is significantly larger

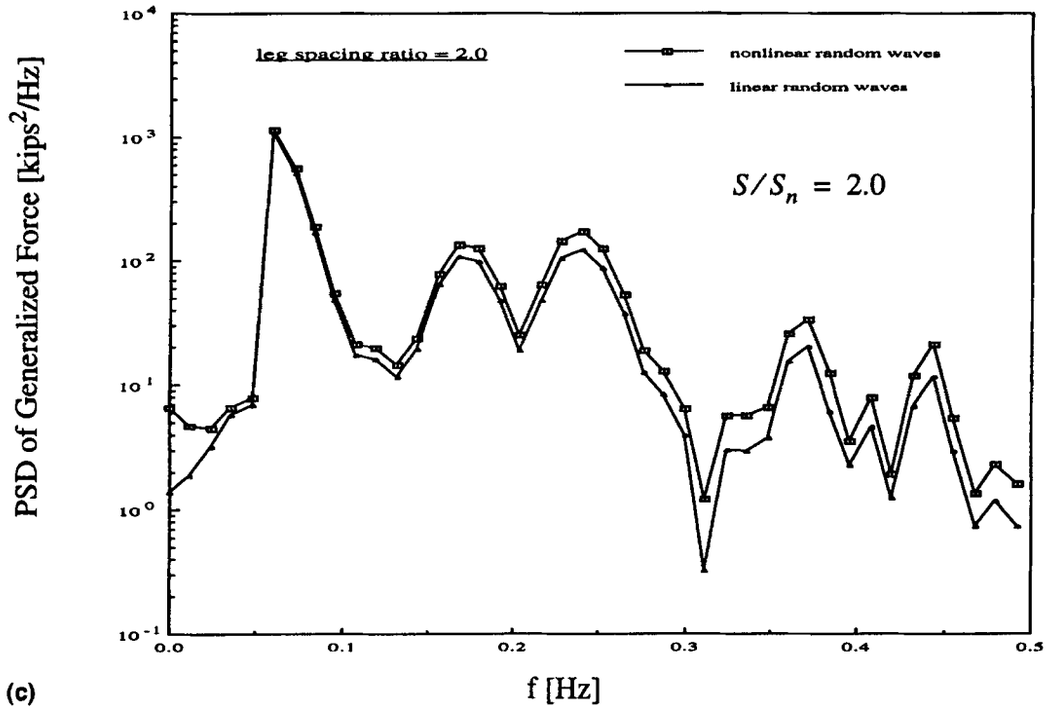

(c)

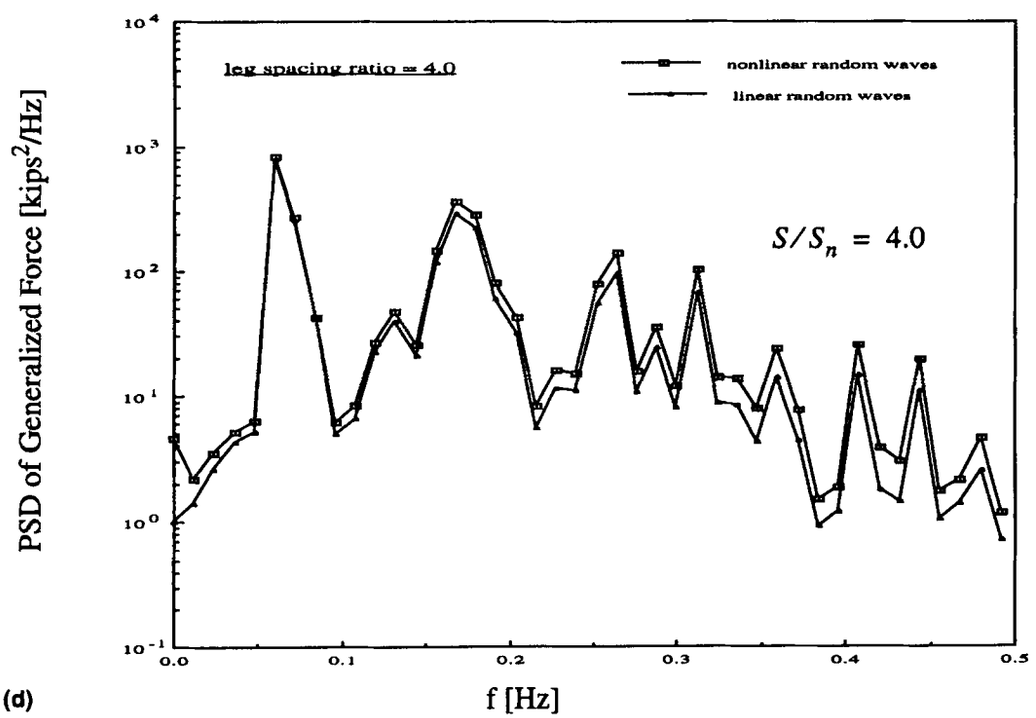

(d)

FIG. 8. (*Continued*)

for an LSR of 4.0. Indeed, as shown in Fig. 8(e), the RMS of deck displacement at an LSR of 4.0 is nearly 50% greater than that at an LSR of 2.0. Furthermore, Fig. 8(e) indicates that the nonlinear analysis provides higher estimates than the linear one. These differences depend on the LSR and vary from 9.1 to 11.7%. Although sea state 3 is not as severe as sea state 2, the magnitude of the deck displacement at any leg configuration based on nonlinear analysis experiences a larger increase in sea state 3 than in sea state 2. This is because the wave nonlinearity produces a larger percentage increase in the RMS of the water-particle velocity for sea state 3 than for sea state 2 (Kareem et al. 1994). In addition, the multimodal nature of sea state 3 increases the significance of the convolution terms in (21)–(24) in the overall response to nonlinear waves. These factors lead to a more significant percentage increase in the RMS of the generalized force on the deck in sea state 3.

CONCLUDING REMARKS

A frequency-domain solution approach for the response of a jacket-type platform whose inputs are Morison forces represented by nonlinear transformations of non-Gaussian wave kinematics has been discussed. It has been shown that this is a more general approach to solution for which the results re-

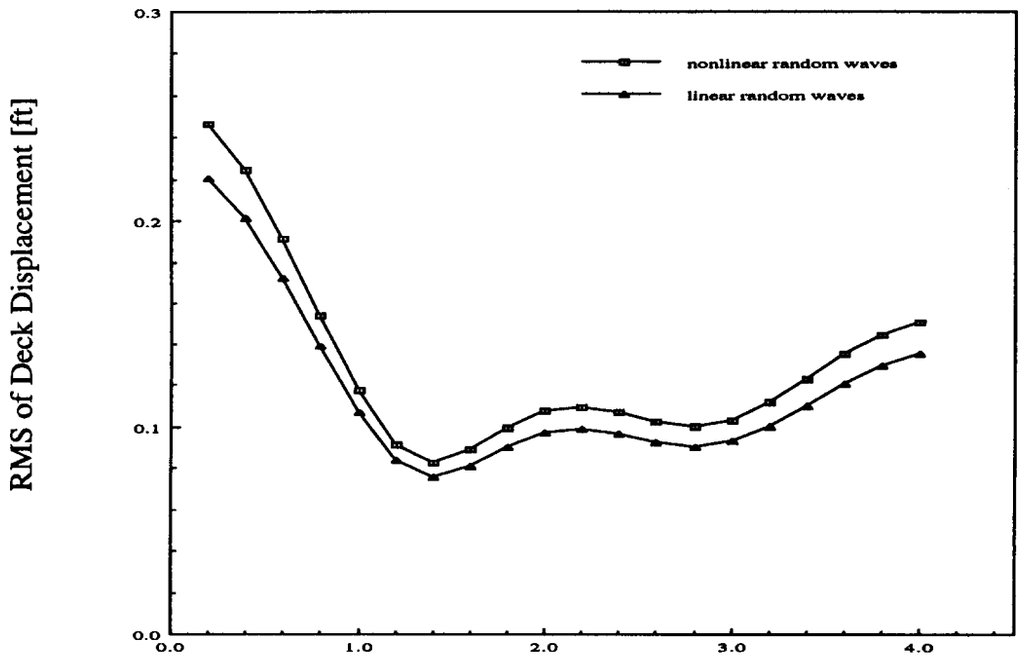

FIG. 8. (*Continued*)

duce, for Gaussian seas, to results published previously. The numerical results indicate that linearization of the drag force may lead to underestimation of the response of the deck in random waves, which reaffirms previously reported studies. Furthermore, it is demonstrated that the displacement level of the deck in nonlinear random waves, for any leg configuration, is larger than for the linear wave theory. This suggests that neglecting wave nonlinearities by utilizing linear wave analysis may result in nonconservative estimates of response statistics, especially in severe seas, or in seas characterized by a combination of low-frequency swells and locally wind-generated waves. Although the contributions of higher response modes are not treated in this study, it is important to note that their possible significance will depend on platform characteristics and design sea states. As a final note, it can be concluded that in addition to the wave theories chosen and the treatment of drag nonlinearity, platform leg configuration is an important parameter that influences the deck motion and, thus, when practical, should be selected to take maximum advantage of wave cancellation effects.

APPENDIX I. SPECTRAL AND PROBABILISTIC DESCRIPTIONS OF NONLINEAR WAVE KINEMATICS

Spectral Description of Nonlinear Wave Kinematics

To facilitate the response analysis of an offshore platform in the frequency domain, it is necessary to determine the statistical and spectral contents of the nonlinear wave kinematics. The free-surface elevation is expressed up to the second order as (e.g., Tick 1959; Kareem and Hsieh 1991; and Kareem et al. 1994)

$$\eta(x, t) = \eta^{(1)}(x, t) + \eta^{(2)}(x, t) \tag{26}$$

using Stokes' perturbation to solve the governing Laplace's equation with nonlinear boundary conditions and the Fourier-Stieltjes spectral representation theorem to represent the random processes (e.g., Kareem et al. 1994, 1996). Its autocorrelation may then be given by

$$R_{\eta\eta}(\tau) = E\{[\eta^{(1)}(x, t) + \eta^{(2)}(x, t)] \cdot [\eta^{(1)}(x, t + \tau) + \eta^{(2)}(x, t + \tau)]\} = \int_{-\infty}^{\infty} e^{i\omega\tau} S^{(1)}_{\eta\eta}(\omega)\, d\omega + \int_{-\infty}^{\infty}\int \frac{2}{g^2} H^2(\omega, \tilde{\omega}) S^{(1)}_{\eta\eta}(\omega) S^{(1)}_{\eta\eta}(\tilde{\omega}) e^{i(\omega+\tilde{\omega})\tau}\, d\omega\, d\tilde{\omega} \tag{27}$$

where $H(\omega, \tilde{\omega}) = (\omega + \tilde{\omega})G(\omega, \tilde{\omega}) + 1/2[|\omega|\omega + \omega\tilde{\omega} - (\omega^2 + \tilde{\omega}^2)]$, $G(\omega, \tilde{\omega}) = (\omega + \tilde{\omega})(\omega\tilde{\omega} - |\omega\tilde{\omega}|)/[(\omega + \tilde{\omega})^2 - \|\omega|\omega + |\tilde{\omega}|\tilde{\omega}|]$, and $E[\cdot]$ is the expectation operator. The convenient features of expectations of products of Gaussian random variables have been utilized in the foregoing equations (e.g., Isserlis 1918) in dealing with the products of processes represented via Fourier-Stieltjes integrals. The PSD of wave elevation follows as:

$$S_{\eta\eta}(\lambda) = S^{(1)}_{\eta\eta}(\lambda) + \int_{-\infty}^{\infty} \frac{1}{2g^2} [|\omega|\omega + |\lambda - \omega|(\lambda - \omega)]^2 \cdot S^{(1)}_{\eta\eta}(\omega) S^{(1)}_{\eta\eta}(\lambda - \omega)\, d\omega \tag{28}$$

where $S^{(1)}_{\eta\eta}(\lambda)$ = first-order wave elevation spectrum (i.e., the wave elevation power spectrum we have chosen to represent our sea state). It is worth pointing out that the free-surface elevation (up to the second order) based on this theory is skewed positively, which is in accordance with observations made concerning ocean waves (e.g., Longuet-Higgins 1963).

Similarly, the first- and second-order terms, correlations, and PSDs of water-particle velocity and acceleration can be obtained (Kareem and Hsieh 1991). The cross-PSD function of water-particle velocity may be written as

$$S_{VV}(x_1, z_1; x_2, z_2; \lambda) = \lambda^2 e^{i|\lambda|\lambda(x_1 - x_2)/g} e^{\lambda^2(z_1 + z_2)/g} S^{(1)}_{\eta\eta}(\lambda) + \int_{-\infty}^{\infty} \frac{D(\omega, \omega - \lambda)}{g^2} e^{i[|\omega|\omega + |\lambda - \omega|(\lambda - \omega)](x_1 - x_2)/g} \cdot e^{\|\omega|\omega + |\lambda - \omega|(\lambda - \omega)|(z_1 + z_2)/g} S^{(1)}_{\eta\eta}(\omega) S^{(1)}_{\eta\eta}(\lambda - \omega)\, d\omega \tag{29}$$

where $D(\omega, \tilde{\omega}) = I^2(\omega, \tilde{\omega}) + I(\omega, \tilde{\omega})I(\tilde{\omega}, \omega)$ and $I(\omega, \tilde{\omega}) = (|\omega|\omega + |\tilde{\omega}|\tilde{\omega})G(\omega, \tilde{\omega})$. When $x_1 = x_2 = x$ and $z_1 = z_2 = z$, the PSD of the water-particle velocity is given by

$$S_{vv}(x, z; \lambda) = \lambda^2 e^{2\lambda^2 z/g} S_{\eta\eta}^{(1)}(\lambda) + \int_{-\infty}^{\infty} \frac{\hat{D}(\omega, \lambda)}{g^2} e^{2\lambda^2(\lambda-2\omega)^2 z/g} S_{\eta\eta}^{(1)}(\omega) S_{\eta\eta}^{(1)}(\lambda - \omega)\, d\omega \tag{30}$$

with

$$\hat{D}(\omega, \lambda) = \begin{cases} 0 & \lambda \geq 0 \text{ and } 0 \leq \omega \leq \lambda \\ 0 & \lambda \leq 0 \text{ and } \lambda \leq \omega \leq 0 \\ 2[\lambda(\lambda - \omega)(\lambda - 2\omega)]^2 & \text{otherwise} \end{cases} \tag{31}$$

The cross-PSD function for water-particle acceleration is given by

$$\begin{aligned} S_{AA}(x_1, z_1; x_2, z_2; \lambda) &= \lambda^4 e^{i|\lambda|\lambda(x_1 - x_2)/g} e^{\lambda^2(z_1 + z_2)/g} S_{\eta\eta}^{(1)}(\lambda) \\ &+ \int_{-\infty}^{\infty} \frac{1}{g^2} N(\omega, \lambda - \omega) e^{\|\omega|\omega + |\lambda - \omega\|(z_1 + z_2)/g} \\ &+ J(\omega, \lambda - \omega)[\omega^3|\lambda - \omega| + (\lambda - \omega)^3|\omega|] \\ &\cdot e^{\{\|\omega|\omega + |\lambda - \omega|(\lambda - \omega)|z_1 + [\omega^2 + (\lambda - \omega)^2]z_2\}/g} \\ &+ 2|\omega|(\lambda - \omega)^3 J(\omega, \lambda - \omega) e^{[(2\omega^2 - 2\lambda\omega + \lambda^2)z_1 + \|\omega|(\lambda - \omega) + |\lambda - \omega|(\lambda - \omega)|z_2]/g} \\ &+ [\omega^2(\lambda - \omega)^6 + \omega^3(\lambda - \omega)^3|(\lambda - \omega)|] e^{[\omega^2 + (\lambda - \omega)^2](z_1 + z_2)/g}\} \\ &\cdot e^{i(\|\omega|\omega + |\lambda - \omega|(\lambda - \omega))/g} S_{\eta\eta}^{(1)}(\omega) S_{\eta\eta}^{(1)}(\lambda - \omega)\, d\omega \end{aligned} \tag{32}$$

where $N(\omega, \lambda - \omega) = J^2(\omega, \lambda - \omega) + J(\omega, \lambda - \omega)J(\lambda - \omega, \omega)$; $J(\omega, \tilde{\omega}) = (\omega + \tilde{\omega})I(\omega, \tilde{\omega})$. The spectrum of water-particle acceleration at a point (x, z) can be obtained simply by setting $x_1 = x_2 = x$ and $z_1 = z_2 = z$ in (32), and the variances of both the water-particle velocity and acceleration $\sigma_V^2(z)$, $\sigma_A^2(z)$ can be obtained by integrating the respective spectra.

Probabilistic Representation of Nonlinear Wave Kinematics

The inclusion of second-order (quadratic) terms renders the probabilistic structure of the water-particle velocity and acceleration non-Gaussian. Considering the nonlinearities of waves in deep water to be weak, the departure of the water-particle velocity and acceleration from Gaussian will be small. Accordingly, the water-particle velocity and acceleration can be expressed in terms of a Hermite series expansion using a functional transformation (e.g., Grigoriu 1995; Winterstein 1985). Let $\bar{V}(x, z, t)$ denote the standardized form of the water-particle velocity process, i.e.

$$\bar{V}(x, z, t) = \frac{V(x, z, t) - E[V(x, z, t)]}{\sigma_V(z)} \tag{33}$$

Utilizing the Hermite series expansion, $\bar{V}(x, z, t)$ can be expressed as

$$\bar{V}(x, z, t) = U_V(x, z, t) + \frac{\alpha_3}{3!}[U_V^2(x, z, t) - 1] + \frac{(\alpha_4 - 3)}{4!}[U_V^3(x, z, t) - 3U_V(x, z, t)] + \cdots \tag{34}$$

where $U_V(x, z, t)$ = standardized form of the first-order water-particle velocity; and coefficients α_3 and α_4, which are the moments of $\bar{V}(x, z, t)$, are defined by $\alpha_3 = E[\bar{V}^3(x, z, t)]$ and $\alpha_4 = E[\bar{V}^4(x, z, t)]$. The preceding series representation of $\bar{V}(x, z, t)$ is truncated after the first few terms (depending on the characteristics of the moments). For convenience in notation, $\alpha_{\bar{V}}(z)$ will be used hereafter in place of $\alpha_3/3!$ and it is given by

$$\begin{aligned} \alpha_{\bar{V}}(z) &= \frac{1}{3!} E[\bar{V}^3(x, z, t)] \\ &= \frac{2}{g\sigma_V^3(z)} \left[\iint_{\text{Ar.3}} \omega_1\omega_2^2(\omega_2^2 - \omega_1^2) e^{2\omega_2^2 z/g} S_{\eta\eta}^{(1)}(\omega_2)\, d\omega_1\, d\omega_2 \right. \\ &+ \left. \iint_{\text{Ar.4}} \omega_1^2\omega_2(\omega_2^2 - \omega_1^2) e^{2\omega_1^2 z/g} S_{\eta\eta}^{(1)}(\omega_1) S_{\eta\eta}^{(1)}(\omega_2)\, d\omega_1\, d\omega_2 \right] \end{aligned} \tag{35}$$

where Ar.3 = an integration area in the $\omega_1 - \omega_2$ plane, bounded by the ω_2-axis and the line $\omega_2 = -\omega_1$; and Ar.4 = an integration area in the same plane, bounded by the ω_1-axis and the line $\omega_2 = -\omega_1$. It is noticed that $\alpha_{\bar{V}}(z)$ remains less than zero because the integrands in both integrals in (35) are always negative.

In a similar manner, a Hermite series representation for the water-particle acceleration can be obtained. Let $\bar{A}(x, z, t)$ describe the standardized water-particle acceleration. Subsequently, an application of the Hermite series expansion of $\bar{A}(x, z, t)$ results in

$$\bar{A}(x, z, t) = U_A(x, z, t) + \frac{\alpha_3}{3!}[U_A^2(x, z, t) - 1] + \frac{(\alpha_4 - 3)}{4!}[U_A^3(x, z, t) - 3U_A(x, z, t)] + \cdots \tag{36}$$

where $U_A(x, z, t)$ = standardized form of the first-order water-particle acceleration. It can be shown that α_3 vanishes, but it is necessary to evaluate the kurtosis α_4. For convenience, the reduced kurtosis $\alpha_{\bar{V}}(z)$ will be used hereafter in place of $(\alpha_4 - 3)/4!$. Expanding the polynomial expression in the foregoing equation and using the derived second-order expression for the water-particle acceleration while neglecting the higher order term $E[A^{(2)}]^4$, yields

$$\begin{aligned} \alpha_{\bar{A}}(z) &= \frac{E\{[A^{(1)}]^3 + 6[A^{(1)}A^{(2)}]^2\} - 3}{24} \\ &= \int_{-\infty}^{\infty} \cdots \int_{-\infty}^{\infty} \frac{1}{g^2\sigma_A^4(z)} [\omega_1^4 J^2(\omega_2, \omega_3) e^{(2\omega_1^2 + 2\|\omega_2|\omega_2 + |\omega_3|\omega_3|)z/g} \\ &+ 4\omega_1\omega_2|\omega_1\omega_2| J(\omega_1, \omega_3)] J(\omega_2, \omega_3) e^{[\omega_1^2 + \omega_2 + \|\omega_2|\omega_2 + |\omega_3|\omega_3| + \|\omega_1|\omega_1 + |\omega_3|\omega_3||z/g} \\ &\cdot S_{\eta\eta}^{(1)}(\omega_1) S_{\eta\eta}^{(1)}(\omega_2) S_{\eta\eta}^{(1)}(\omega_3)\, d\omega_1\, d\omega_2\, d\omega_3 \\ &+ \frac{1}{2g^2\sigma_A^4(z)} \left\{ \int_0^{\infty} \omega^4 e^{2\omega^2 z/g} S_{\eta\eta}^{(1)}(\omega)\, d\omega \left[\iint_{\text{Ar.1}} (\omega_1^3\omega_2^5 - \omega_1^5\omega_2^3 \right. \right. \\ &+ \omega_1^4\omega_2^4 - \omega_1^2\omega_2^6) e^{2(\omega_1^2 + \omega_2^2)z/g} S_{\eta\eta}^{(1)}(\omega_1) S_{\eta\eta}^{(1)}(\omega_2)\, d\omega_1\, d\omega_2 \\ &+ \iint_{\text{Ar.2}} (\omega_1^4\omega_2^4 - \omega_1^2\omega_2^6 - \omega_1^3\omega_2^5 + \omega_1\omega_2^7) \\ &\cdot e^{2(\omega_1^2 + \omega_2^2)z/g} S_{\eta\eta}^{(1)}(\omega_1) S_{\eta\eta}^{(1)}(\omega_2)\, d\omega_1\, d\omega_2 \Big] + \int_0^{\infty} \omega^5 e^{2\omega^2 z/g} S_{\eta\eta}^{(1)}(\omega)\, d\omega \\ &\cdot \left[\iint_{\text{Ar.1}} \omega_1^3\omega^2(\omega_1 - \omega_2)^2(\omega_1 + \omega_2) e^{2(\omega_1^2 + \omega_2^2)z/g} \right. \\ &\cdot S_{\eta\eta}^{(1)}(\omega_1) S_{\eta\eta}^{(1)}(\omega_2)\, d\omega_1\, d\omega_2 - \iint_{\text{Ar.2}} \omega_1^2\omega_2^2(\omega_1 - \omega_2)^2(\omega_1 + \omega_2) \\ &\cdot \left. \left. e^{2(\omega_1^2 + \omega_2^2)z/g} S_{\eta\eta}^{(1)}(\omega_1) S_{\eta\eta}^{(1)}(\omega_2)\, d\omega_1\, d\omega_2 \right] \right\} \\ &+ \frac{1}{4g^2\sigma_A^4(z)} \int_{-\infty}^{\infty} \cdots \int_{-\infty}^{\infty} (\omega_1^4\omega_2^2\omega_3^6 + 2\omega_1^4\omega_2^4\omega_3^2|\omega_1\omega_2|) \\ &\cdot e^{2(\omega_1^2 + \omega_2^2 + \omega_3^2)z/g} S_{\eta\eta}^{(1)}(\omega_1) S_{\eta\eta}^{(1)}(\omega_2) S_{\eta\eta}^{(1)}(\omega_3)\, d\omega_1\, d\omega_2\, d\omega_3 \end{aligned} \tag{37}$$

where Ar.1 and Ar.2 = integration areas in the $\omega_1 - \omega_2$ plane, respectively, bounded by the ω_1-axis and the line $\omega_2 = \omega_1$ and by the ω_2-axis and the line $\omega_2 = \omega_1$.

ACKNOWLEDGMENTS

This study was supported in part by the Office of Naval Research (ONR) Grant 00014-93-1-0761 and the National Science Foundation (NSF) Grant CMS-95-03779. The third writer also was supported in part by a GAANNP fellowship.

APPENDIX II. REFERENCES

Borgman, L. E. (1965). "The spectral density for ocean wave forces." *Proc., 4th Coast. Engrg. Conf.*, ASCE, New York, N.Y.

Borgman, L. E. (1967). "Random hydrodynamic forces on objects." *Ann. Math. Statist.*, 38, 37–51.

Borgman, L. E. (1982). "Specification of the wave environment." *Proc., Oc. Struct. Dyn. Symp.*, Oregon State Univ., Corvallis, Oreg., 1–27.

Chakrabarti, S. K. (1987). *Hydrodynamics of offshore structures.* Springer-Verlag, Berlin, Germany.

Deleuil, G. E., Des Deserts, L. D., Doris, C. G., and Shive, A. (1986). "A new method for frequency domain analysis of offshore structures: comparison with time domain analysis." *Proc., 18th Offshore Technol. Conf., OTC Paper 5303*, Offshore Technology Conference, Dallas, Tex., 103–110.

Eatock-Taylor, R., and Rajagopalan, A. (1982). "Dynamics of offshore structures, part I: perturbation analysis." *J. Sound and Vibration*, 83(3), 401–416.

Grigoriu, M. (1995). *Applied non-Gaussian processes.* Prentice-Hall, Inc., Englewood Cliffs, N.J.

Gudmestad, O. T., and Connor, J. J. (1983). "Linearization methods and the influence of current on the nonlinear hydrodynamic drag force." *Appl. Oc. Res.*, 5(4), 184–194.

Isserlis, L. (1918). "On a formula for the product-moment coefficient in any number of variables." *Biometrika*, 12(1–2), 134–139.

Kareem, A., and Hsieh, C. C. (1991). "Probabilistic response analysis of offshore platforms to wave loading." *Tech. Rep. No. CEND 91-1*, Dept. of Civ. Engrg., Univ. of Notre Dame, Notre Dame, Ind.

Kareem, A., Hsieh, C. C., and Tognarelli, M. A. (1994). "Response analysis of offshore systems to nonlinear random waves: part I—wave field characteristics." *Proc., 1994 ASME Wint. Ann. Mtg. Spec. Symp. Stoc. Dyn. Rel. Oc. Sys.*, American Society of Mechanical Engineers, New York, N.Y.

Kareem, A., Hsieh, C. C., and Tognarelli, M. A. (1996). "Frequency-domain response analysis of a jacket-type platform in a nonlinear random wave field." *Tech. Rep. No. NDCE 96-003*, Dept. of Civ. Engrg. and Geol. Sci., Univ. of Notre Dame, Notre Dame, Ind.

Kareem, A., and Li, Y. (1992). "Equivalent statistical quadratization of nonlinear hydrodynamic loads on TLPs." *Proc., Int. Conf. on Civ. Engrg. in the Oceans V*, ASCE, New York, N.Y.

Kareem, A., and Zhao, J. (1994). "Analysis of non-Gaussian surge response of tension leg platforms under wind loads." *J. Offshore Mech. Arctic Engrg.*, 116, 137–144.

Kareem, A., Zhao, J., and Tognarelli, M. A. (1995). "Surge response statistics of tension leg platforms under wind and wave loads: a statistical quadratization approach." *Probabilistic Engrg. Mech.*, Essex, U.K., 10(4), 225–240.

Li, Y., and Kareem, A. (1992). "Computation of wind-induced drift forces introduced by displaced position of compliant offshore platforms." *J. Offshore Mech. Arctic Engrg.*, American Society of Mechanical Engineers, 114(August), 175–184.

Lipsett, A. W. (1986). "Nonlinear structural response in random waves." *J. Struct. Engrg. Div.*, ASCE, 112(11), 2416–2429.

Longuet-Higgins, M. S. (1963). "The effect of non-linearities on statistical distributions in the theory of sea waves." *Proc., Royal Soc.*, London, England, 287A, 459–480.

Marthinsen, T., and Winterstein, S. R. (1992). "On the skewness of random surface waves." *Proc., 2nd Int. Offshore and Polar Engrg. Conf.*, International Society of Offshore and Polar Engineers, New York, N.Y., 472–478.

Naess, A., and Yim, S. C. S. (1996). "Stochastic response of offshore structures excited by drag forces." *J. Engrg. Mech.*, ASCE, 122(5), 442–448.

Papoulis, A. (1965). *Probability random variables and stochastic processes.* McGraw-Hill Inc., New York, N.Y.

Price, R. (1958). "A useful theorem for nonlinear devices having Gaussian inputs." *I. R. E. Trans. PGIT*, 4, 69–72.

Rajagopalan, A., and Eatock-Taylor, R. (1982). "Dynamics of offshore structures, part II: stochastic averaging analysis." *J. Sound and Vibration*, 83(3), 417–431.

Sigbjornsson, R., and Morch, M. (1982). "Spectral analysis of nonlinear wave load effects on offshore platforms." *Engrg. Struct.*, 4, 29–36.

Spanos, P. D., and Donley, M. G. (1990). "Stochastic response of a tension leg platform to viscous drift forces." *9th Int. OMAE Conf.*, American Society of Mechanical Engineers, New York, N.Y., 212–218.

Spidsøe, N., and Hilmarsen, B. (1983). "Measured dynamic behavior of North Sea gravity platforms under extreme environmental conditions." *Proc., 15th Offshore Tech. Conf., OTC Paper 4613*, Offshore Technology Conference, Dallas, Tex., 283–300.

Tayfun, M. A. (1990). "High wave number/frequency attenuation of wind-wave spectra." *J. Wtrwy., Port, Coast., and Oc. Engrg.*, ASCE, 116(3), 381–398.

Tick, L. J. (1959). "A non-linear random model of gravity waves I." *J. Mathematics and Mech.*, 8(5), 643–651.

Tognarelli, M. A., Zhao, J., Rao, K. B., and Kareem, A. (1997). "Equivalent statistical quadratization and cubicization for nonlinear systems." *J. Engrg. Mech.*, ASCE, 123(5), 512–523.

Tung, C. C. (1975). "Statistical properties of wave force." *J. Engrg. Mech. Div.*, ASCE, 100(1), 1–11.

Winterstein, S. R. (1985). "Non-normal responses and fatigue damage." *J. Engrg. Mech.*, ASCE, 111(10), 1291–1295.